Check for updates

ChemMedChem

Chemistry Europe
European Chemical Societies Publishing
ChemMedChem

RESEARCH ARTICLE

CD44-Targeted Delivery of Melittin and Celecoxib via Hyaluronic Acid-Coated Polymersomes for Synergistic Anti-Inflammatory Therapy

Youngheun Cho[1] | Junmin Kim[1] | Jooho Moon[1] | Soobin Nam[1] | Junhyung Kim[1] | Hyuncheol Kim[1,2]

[1]Department of Chemical and Biomolecular Engineering, Sogang University, Seoul, Republic of Korea | [2]Department of Biomedical Engineering, Sogang University, Seoul, Republic of Korea

Correspondence: Hyuncheol Kim (hyuncheol@sogang.ac.kr)

Received: 11 December 2025 | **Revised:** 27 June 2026 | **Accepted:** 2 July 2026

Keywords: anti-inflammatory therapy | CD44-targeted drug delivery | hyaluronic acid coating | melittin–celecoxib codelivery | nanoparticles | polymersome

ABSTRACT

Activated macrophages are key effector cells in inflammatory diseases, but the therapeutic use of membrane-active agents such as melittin (MEL) is limited by nonspecific cytotoxicity and hemolysis. Here, we developed a hyaluronic acid (HA)-coated MEL-based polymersome (PMHA) for CD44-targeted codelivery of MEL and celecoxib (CXB). MEL was incorporated into the vesicular membrane, whereas CXB was loaded into the hydrophobic domain. PMHA showed a hydrodynamic diameter of 265.5 ± 1.6 nm, a zeta-potential of −21.14 ± 1.1 mV, a CXB encapsulation efficiency of 70.81 ± 4.18%, and a drug loading capacity of 12.87 ± 1.92%. In lipopolysaccharide (LPS)-stimulated RAW 264.7 macrophages, anti-CD44 antibody blocking reduced Alexa Fluor 647-labeled PMHA uptake by approximately 37.5%, supporting HA–CD44-mediated internalization. PMHA reduced MEL-associated cytotoxicity and hemolytic activity and enabled pH-responsive CXB release. Codelivery of MEL and CXB suppressed cyclooxygenase-2 (COX-2) and tumor necrosis factor-α (TNF-α) expression, with combination index (CI) values of 0.48 and 0.67, respectively. These findings support further evaluation of PMHA as a macrophage-targeted anti-inflammatory nanoplatform.

1 | Introduction

Inflammation is a complex biological defense mechanism triggered by tissue injury or microbial invasion. It involves the activation of immune cells and the release of proinflammatory cytokines, including tumor necrosis factor-α (TNF-α), interleukin-1β (IL-1β), and interleukin-6 (IL-6) [1, 2]. While acute inflammation is essential for host defense and tissue repair, its dysregulation can lead to chronic inflammatory diseases such as cardiovascular disease, neurodegenerative disorders, and autoimmune conditions [3]. Accordingly, therapeutic strategies that modulate inflammatory signaling and cytokine production have gained increasing attention [4]. The RAW 264.7 macrophage cell line treated with lipopolysaccharide (LPS) serves as a well-established in vitro model for evaluating anti-inflammatory agents [5, 6]. LPS, a major component of Gram-negative bacterial membranes, activates Toll-like receptor 4 (TLR4), leading to downstream activation of nuclear factor-kappa B (NF-κB) and mitogen-activated protein kinases (MAPKs) [7]. This cascade induces the expression of inducible nitric oxide synthase (iNOS) and cyclooxygenase-2 (COX-2), resulting in elevated levels of nitric oxide (NO), prostaglandin E_2 (PGE_2), and cytokines, thereby recapitulating key features of acute inflammation [8]. Melittin (MEL), a 26-amino acid amphiphilic peptide derived from bee venom, exhibits potent anti-inflammatory activity by inhibiting NF-κB activation and suppressing iNOS and COX-2 expression [9–11]. However, its therapeutic application is limited by nonspecific membrane-disruptive effects and cytotoxicity, which can cause hemolysis and tissue damage at pharmacological concentrations [12]. Nanoparticle-based delivery platforms, such as polymersomes and lipid nanoparticles, have been employed to enhance targeting specificity and reduce systemic toxicity [13, 14]. Celecoxib

All rights reserved, including rights for text and data mining and training of artificial intelligence technologies or similar technologies.
© 2026 Wiley-VCH GmbH.

(CXB), a selective COX-2 inhibitor, provides a complementary anti-inflammatory mechanism by attenuating prostanoid biosynthesis [15]. Despite its improved gastrointestinal safety profile over nonselective NSAIDs, CXB suffers from poor aqueous solubility and requires high doses to achieve therapeutic efficacy, which can result in hepatotoxicity and cardiovascular complications with long-term use [16]. To overcome these challenges, advanced delivery systems are needed to improve CXB's bioavailability and enable selective delivery to inflamed tissues. Codelivery of MEL and CXB within a single nanoparticle system represents a rational therapeutic approach that enables complementary modulation of distinct inflammatory pathways while minimizing the dose-limiting toxicities of each agent. To further enhance site-specific delivery, a HA-coated MEL-based polymersome (PMHA) was developed by incorporating hyaluronic acid (HA), a biocompatible and biodegradable glycosaminoglycan. HA binds to CD44, a receptor highly expressed on activated macrophages under inflammatory conditions [17–19], facilitating receptor-mediated uptake of nanoparticles at inflamed sites while reducing off-target distribution [20, 21]. Previous studies have demonstrated the feasibility of HA as a targeting head for inflammatory cell-directed delivery. For example, Zhang et al. reported that hyaluronan-modified ethosomes enhanced the topical antipsoriatic efficacy of curcumin through CD44-assisted drug clustering in inflammatory skin [22].

The engineered PMHA was designed to enable CD44-mediated targeting, facilitate selective delivery to activated macrophages, and exert anti-inflammatory effects through the combined actions of melittin and celecoxib. This nanoplatform is expected to enhance the therapeutic potential of both agents and offers a rational strategy for the treatment of macrophage-mediated inflammatory diseases.

2 | Materials and Methods

2.1 | Materials

HA (average molecular weight 10 kDa; product code HA-101) was purchased from Creative PEGWorks (Chapel Hill, NC, USA). Dimethyl sulfoxide (DMSO), dichloromethane (DCM), and general laboratory reagents were obtained from Sigma–Aldrich (St. Louis, MO, USA). Poly(D,L-lactide)-NHS ($M_n \approx 7$ kDa) (PDLLA-NHS) was purchased from Ruixibiotech (Xi'an, China). Celecoxib (CXB) and 2-(pyridyldithio)ethylamine hydrochloride were purchased from MedChemExpress (Monmouth Junction, NJ, USA). Reduced glutathione was obtained from FUJIFILM Wako (Richmond, VA, USA). Alexa Fluor 488-conjugated anti-mouse/human CD44 antibody was purchased from BioLegend (San Diego, CA, USA). Alexa Fluor 647 NHS Ester (succinimidyl ester; Cat# A20006) was purchased from Invitrogen/Thermo Fisher Scientific (Waltham, MA, USA). A cysteine-modified melittin peptide (C-Cys-MEL) was synthesized by GenScript Biotech (Piscataway, NJ, USA). Mouse red blood cells (RBCs) were purchased from Innovative Research (Novi, MI, USA). RPMI 1640 medium, fetal bovine serum (FBS), and antibiotic–antimycotic (AA) solution were purchased from Welgene (Gyeongsan, Republic of Korea).

2.2 | Preparation of PM and PMHA

PM were synthesized through a two-step procedure involving polymer–linker conjugation and peptide activation. First, PDLLA–NHS was reacted with 2-(pyridyldithio)ethylamine hydrochloride in anhydrous dichloromethane (DCM) under a nitrogen atmosphere for 24 h. The resulting polymer–linker was purified by dialysis (molecular weight cutoff: 2 kDa) against deionized water. For peptide activation, C-Cys-MEL was reduced with tris(2-carboxyethyl)phosphine (TCEP), followed by centrifugal filtration using a 3 kDa MWCO filter at 4000 × *g* and 25°C for 10 min, repeated 5 times, to remove excess reagent. Sulfhydryl content was quantified using Ellman's reagent. The activated peptide was then conjugated to the polymer–linker via a disulfide exchange reaction in a DCM/DMSO/water mixture (1:10:1, v/v/v). The resulting PM were further purified by dialysis, and unreacted components were removed by DCM extraction. For peptide quantification, 1% Triton X-100 was added, and a fluorescamine assay was subsequently conducted [23]. For drug loading, CXB was dissolved in anhydrous DCM and added dropwise into the preformed PM dispersion under magnetic stirring. The mixture was stirred to allow CXB incorporation into the hydrophobic domains of PM, followed by solvent evaporation under reduced pressure. The resulting dispersion was centrifuged at 4000 × *g* and 25°C for 10 min, and the pellet containing CXB-loaded PM was collected. The supernatant was analyzed by high-performance liquid chromatography (HPLC) to quantify nonencapsulated CXB. To prepare PMHA, the CXB-loaded PM dispersions were subsequently mixed with HA at a mass ratio of 1:2 (PM: HA, w/w) and incubated at room temperature for 6 h to facilitate surface adsorption via electrostatic interaction.

The encapsulation efficiency (EE) and drug loading capacity (DLC) of CXB were calculated using Equations (1) and (2), respectively. For EE determination, an aliquot of the PMHA dispersion was completely disrupted with 0.1% (v/v) Triton X-100 to determine the total CXB concentration. A separate aliquot was diluted 10-fold in PBS without Triton X-100 to determine the non-encapsulated CXB concentration. All measured concentrations were corrected for dilution factors before calculation.

$$\mathrm{EE}\,(\%) = \frac{C_{\mathrm{Triton}} - C_{\mathrm{PBS}}}{C_{\mathrm{Triton}}} \times 100 \tag{1}$$

$$\mathrm{DLC}\,(\%) = \frac{W_{\mathrm{CXB,loaded}}}{W_{\mathrm{CXB\text{-}loaded\ PMHA}}} \times 100 \tag{2}$$

where C_{Triton} is the total CXB concentration measured after complete disruption of PMHA with 0.1% (v/v) Triton X-100, and C_{PBS} is the dilution-corrected CXB concentration measured in the 10-fold diluted PBS sample without Triton X-100, representing non-encapsulated CXB. $W_{\mathrm{CXB,loaded}}$ is the amount of CXB encapsulated in PMHA, calculated from the difference between C_{Triton} and C_{PBS}, and $W_{\mathrm{CXB\text{-}loaded\ PMHA}}$ is the total dry mass of the CXB-loaded PMHA formulation.

2.3 | Preparation of Fluorescently Labeled PMHA

Fluorescently labeled PMHA was prepared by covalently conjugating Alexa Fluor 647-NHS ester to surface-exposed primary amine groups of PM. Briefly, PM dispersion in PBS was mixed with Alexa Fluor 647-NHS ester at a molar ratio of Alexa

18607187, 2026, 14, Downloaded from https://chemistry-europe.onlinelibrary.wiley.com/doi/10.1002/cmdc.70396 by Hyuncheol Kim - Sogang University , Wiley Online Library on [24/07/2026]. See the Terms and Conditions (https://onlinelibrary.wiley.com/terms-and-conditions) on Wiley Online Library for rules of use; OA articles are governed by the applicable Creative Commons License

Fluor 647-NHS ester:surface primary amine = 1:1 and reacted for 3 h at 25°C in the dark. Unreacted dye was removed by centrifugal filtration at 4000 × *g* and 25°C for 10 min, repeated twice. The Alexa Fluor 647-labeled PM was then coated with HA at a mass ratio of 1:2 (PM:HA, w/w) for 6 h at room temperature, as described above, to obtain fluorescently labeled PMHA. The concentration of unreacted dye was quantified by fluorescence spectroscopy using a calibration curve of Alexa Fluor 647 NHS Ester, with excitation and emission wavelengths of approximately 650 and 668 nm, respectively. The labeling efficiency was calculated using Equation (3):

$$\text{Labeling efficiency}\,(\%) = \frac{C_{\text{dye},0} - C_{\text{dye,free}}}{C_{\text{dye},0}} \times 100 \qquad (3)$$

where $C_{\text{dye},0}$ is the initial concentration of Alexa Fluor 647-NHS ester added to the reaction mixture, and $C_{\text{dye,free}}$ is the concentration of unreacted dye detected after purification. The labeling efficiency of Alexa Fluor 647 was 72.1 ± 4.8%.

2.4 | Characterization of PM and PMHA

The hydrodynamic diameter and zeta potential of PM and PMHA were measured using dynamic light scattering (DLS) (Zetasizer Nano ZS, Malvern Instruments, Herrenberg, Germany). For TEM analysis, 5 μL of diluted nanoparticle suspension was deposited onto a 200-mesh carbon-coated copper grid and allowed to adsorb for 1 min. Excess sample was removed with filter paper, and the grid was negatively stained with 1% uranyl acetate for 30 s. After air-drying at room temperature, samples were imaged using a JEM-2100F transmission electron microscope (JEOL, Tokyo, Japan) operated at 200 kV.

2.5 | In Vitro Drug Release Studies

The release profile of CXB from PMHA was evaluated under both physiological and endosomal/lysosomal pH conditions using reverse-phase high-performance liquid chromatography (RP-HPLC; Nexera Lite PDA, Shimadzu, Japan). Regenerated cellulose dialysis membranes with a molecular weight cutoff of 3.5 kDa were used. PMHA dispersed in 1 mL of phosphate-buffered saline (PBS, pH 7.3 or pH 5.0) were loaded into dialysis bags and sealed. The bags were immersed in 50 mL of PBS and maintained at 37°C under continuous shaking (120 rpm). Samples (5 mL) of the release medium were collected at predefined time points (1, 3, 5, 7, 12, 24, and 48 h), and the volume was replaced with fresh PBS after each sampling. CXB concentrations in the collected samples were quantified using an RP-HPLC system equipped with a ZORBAX Eclipse XDB-C18 column (250 mm × 4.6 mm, 5 μm particle size). The mobile phase consisted of 85% methanol with 0.01% trifluoroacetic acid (TFA) and 15% water with 0.01% TFA. The flow rate was set to 0.8 mL/min, and detection was performed at 251 nm with a column temperature of 40°C and an injection volume of 5 μL. Each run was maintained for 30 min.

2.6 | Cell Culture

RAW 264.7 murine macrophage-like cells were obtained from the Korean Cell Line Bank (KCLB, Seoul, Republic of Korea; KCLB Cat # 40 071, RRID: CVCL_0493). Cells were cultured in RPMI 1640 medium supplemented with 10% fetal bovine serum and 1% antibiotic–antimycotic solution at 37°C in a humidified atmosphere containing 5% CO_2.

2.7 | In Vitro Cytotoxicity Assay

The cytotoxicity of MEL and PMHA was assessed using the MTT assay. RAW 264.7 cells were seeded in 96-well plates at a density of 1.0×10^4 cells per well in 100 μL of complete medium and incubated overnight. The following day, cells were treated with MEL or PMHA (equivalent MEL concentrations of 0.5, 1, and 2 μg/mL) in serum-free medium and incubated for 24 h. After treatment, the medium was removed, and 50 μL of MTT solution (1 mg/mL in PBS) was added to each well. Plates were incubated for an additional 3 h at 37°C. Following incubation, the resulting formazan crystals were dissolved in 150 μL of DMSO, and the plates were shaken for 30 min to ensure complete dissolution. Absorbance was measured at 570 nm with a reference wavelength of 650 nm using a microplate reader (Bio-Tek, USA). Untreated cells served as the control group, and all experiments were conducted in triplicate.

2.8 | Hemolysis Assay of MEL and PMHA

Hemolytic activity of MEL and PMHA was evaluated using mouse red blood cells (RBCs). RBCs were diluted to a final concentration of 5.0×10^7 cells/mL. To assess hemolysis, 100 μL of the diluted RBC suspension was incubated with varying concentrations of MEL (0.5–10 μg/mL), either as free MEL or as MEL in PMHA, at 37°C for 6 h. Following incubation, samples were centrifuged at 3000 × g for 5 min, and the absorbance of the supernatant was measured at 450 nm using a microplate reader to determine the extent of hemoglobin release. Distilled water and PBS were used as positive and negative controls, respectively.

2.9 | In Vitro Flow Cytometry and Cellular Uptake Imaging

Flow cytometry analysis was performed using a FACS Aria II system (BD Biosciences, New Jersey, USA). RAW 264.7 macrophages were seeded in 12-well plates at a density of 1.0×10^5 cells/mL and incubated for 12 h at 37°C. To block CD44 receptors, cells were treated with Alexa Fluor 488-conjugated anti-mouse/human CD44 antibody (1 μg/mL) and incubated for an additional 12 h. After washing with Dulbecco's phosphate-buffered saline (DPBS), Alexa Fluor 647-labeled PMHA (equivalent to 2 μg/mL MEL in serum-free medium) were added to the CD44-blocked cells and incubated for 24 h at 37°C. Cellular uptake and CD44-mediated targeting were assessed by flow cytometry. For qualitative imaging, confocal laser scanning microscopy was used (LSM 5 PASCAL, Carl Zeiss, Germany). Cells were prepared as described above, except that they were seeded in confocal dishes. After incubation with dye-labeled PMHA, cells were fixed with 4% paraformaldehyde and stained with 4′,6-diamidino-2-phenylindole (DAPI) to visualize nuclei. Samples were imaged using confocal microscopy.

18607187, 2026, 14, Downloaded from https://chemistry-europe.onlinelibrary.wiley.com/doi/10.1002/cmdc.70396 by Hyuncheol Kim - Sogang University , Wiley Online Library on [24/07/2026]. See the Terms and Conditions (https://onlinelibrary.wiley.com/terms-and-conditions) on Wiley Online Library for rules of use; OA articles are governed by the applicable Creative Commons License

2.10 | In Vitro Gene Expression

The mRNA expression levels of TLR-4, COX-2, and TNF-α were evaluated by reverse transcription polymerase chain reaction (RT-PCR). RAW 264.7 cells were seeded in 12-well plates at a density of 1.0×10^5 cells/mL and incubated for 12 h at 37°C. Cells were then treated with MEL or PMHA at MEL-equivalent concentrations of 0.5, 1, or 2 μg/mL in serum-free medium for 24 h. Total RNA was extracted using the AccuPrep Universal RNA Extraction Kit (Bioneer, Daejeon, Republic of Korea). One-step RT-PCR was conducted using the AccuPower RT/PCR PreMix (Bioneer) according to the manufacturer's instructions. PCR products were separated on 2% agarose gels by electrophoresis at 75 V for 45 min.

The following primers were used:

GAPDH forward: 5′-ATGGGTGTGAACCACGAGA-3′

GAPDH reverse: 5′-GGAGAGACTATCAAGATAGT-3′

TLR4 forward: 5′-CTGGTGGCTGTGGAGACAAA-3′

TLR4 reverse: 5′-GGATGATGTTGGCAGCAATGG-3′

COX2 forward: 5′-CACTACATCCTGACCCACTT-3′

COX2 reverse: 5′-ATGCTCCTGCTTGAGTATGT-3′

TNF forward: 5′-CAGAAAGCATGATCCGCGAC-3′

TNF reverse: 5′-TTGGGCAGATTGACCTCAGC-3′

2.11 | Quantification of Inflammatory Mediators by ELISA

For inflammatory mediator quantification, RAW 264.7 macrophages were seeded in 24-well plates at a density of 1×10^5 cells/well and allowed to adhere overnight. Cells were pretreated with various formulations at the indicated concentrations: PMHA (0.25–2 μg/mL, based on melittin content) and CXB (0.25–1 μg/mL) for the dose–response study. The levels of COX-2 and TNF-α were then measured by ELISA, as shown in Figure S1a,b, respectively. For combination studies , the concentrations were fixed at 2 μg/mL for PMHA (melittin equivalent) and 1 μg/mL for CXB. After 24 h of pretreatment, cells were treated with LPS (1 μg/mL) for 12 h. Supernatants were collected and centrifuged at 3000 × *g* for 10 min to remove debris. The concentrations of TNF-α and COX-2 were quantified using commercial ELISA kits [TNF-α: Abcam, ab208348; COX-2: Abcam, ab210574] according to the manufacturer's instructions. Absorbance was measured at 450 nm using a microplate reader (SpectraMax, Molecular Devices), and analyte concentrations were calculated from standard curves.

2.12 | Combination Index Analysis

The dose–response relationship of each drug was analyzed according to the median-effect principle described by Chou and Talalay [24]. The fraction affected (F_a) was calculated using Equation (4):

$$F_a = \frac{(E_{LPS} - E_{treatment})}{(E_{LPS} - E_{control})} \tag{4}$$

where E_{LPS} is the mean response in the LPS-treated group, $E_{control}$ is the response in the control group, and $E_{treatment}$ is the response in the drug-treated group. In this study, F_a represents the fractional inhibition of inflammatory mediator expression relative to the LPS-induced response.

The median-effect equation was applied using Equation (5):

$$\frac{F_a}{1 - F_a} = \left(\frac{D}{D_m}\right)^m \tag{5}$$

where D is the drug dose, D_m is the median-effect dose, and m is the slope of the median-effect plot. The values of D_m and m were determined from the dose–response curves of each single treatment.

For drug combinations, the combination index (CI) was calculated using Equation (6):

$$CI = \frac{D_1}{D_{x1}} + \frac{D_2}{D_{x2}} \tag{6}$$

where D_1 and D_2 are the doses of the combined drugs producing a given effect, and D_{x1} and D_{x2} are the doses of each drug alone that achieve the same effect. CI values were interpreted as follows: $CI < 1$ indicates synergism, $CI = 1$ indicates additivity, and $CI > 1$ indicates antagonism.

2.13 | Statistical Analysis

All biological experiments were conducted independently at least three times unless otherwise stated. Data are presented as mean ± standard deviation (SD). Data normalization was performed as described in each assay, and no additional data transformation or outlier exclusion was applied. Statistical analyses were performed using Origin 2021 (OriginLab Corporation, Northampton, MA, USA). For two-group comparisons, a two-sided unpaired Student's t-test was used. For concentration-dependent comparisons between free MEL and PMHA, two-way analysis of variance (ANOVA) followed by Sidak's multiple-comparisons test was used. For comparisons involving multiple treatment groups, one-way ANOVA followed by Tukey's multiple-comparisons test was used. A *p*-value less than 0.05 was considered statistically significant. Significance levels are indicated as follows: ns, not significant; $*p < 0.05$; $**p < 0.01$; $***p < 0.001$.

2.14 | Results and Discussion

2.14.1 | Design and Synthesis of HA-Coated Nanoparticles for Inflammation-Targeted Therapy

PM were engineered by conjugating hydrophobic PDLLA with C-Cys-MEL, resulting in an amphiphilic copolymer that spontaneously self-assembled into vesicular nanostructures. The disulfide linkage between PDLLA and MEL provided redox responsiveness, enabling glutathione-triggered cleavage and intracellular release of the therapeutic peptide. Vesicle formation is strongly governed

18607187, 2026, 14, Downloaded from https://chemistry-europe.onlinelibrary.wiley.com/doi/10.1002/cmdc.70396 by Hyuncheol Kim - Sogang University , Wiley Online Library on [24/07/2026]. See the Terms and Conditions (https://onlinelibrary.wiley.com/terms-and-conditions) on Wiley Online Library for rules of use; OA articles are governed by the applicable Creative Commons License

by the molecular weight balance between hydrophilic and hydrophobic segments; polymersomes are typically formed when the hydrophilic block comprises 25%–40% of the total molecular weight [25]. In this system, MEL and low-molecular-weight PDLLA were combined to satisfy this criterion and promote bilayer formation in aqueous solution. To impart inflammation-targeting capability, HA was electrostatically adsorbed onto the surface of PM, forming PMHA. HA serves as a ligand for CD44 receptors, which are overexpressed on activated macrophages in inflamed tissues [21]. DLS revealed an increase in hydrodynamic diameter from 218.2 ± 1.7 nm for PM to 265.5 ± 1.6 nm for PMHA (Figure 1a), consistent with the presence of an HA corona. In addition, zeta-potential measurements showed a surface charge reversal from +24.67 mV to −21.14 mV following HA coating (Figure 1b), confirming successful deposition of the anionic polyelectrolyte. The observed electrostatic inversion serves as a key indicator of successful polyelectrolyte adsorption and contributes to the prevention of nanoparticle aggregation near the isoelectric point [26]. Optimization experiments identified a 1:2 PM-to-HA (w/w) mass ratio as optimal for colloidal stability, as higher HA concentrations led to visible aggregation (Table 1). TEM confirmed the hollow, bilayered morphology of PM. Upon HA coating, the membrane of PMHA appeared thicker and darker, in line with HA adsorption and consistent with previously reported HA-coated vesicular systems (Figure 1c) [27].

2.14.2 | *Drug Loading and In Vitro Release Profile*

CXB was successfully incorporated into PMHA, with an encapsulation efficiency of 70.81 ± 4.18% and a drug loading capacity of 12.87 ± 1.92%. These results indicate that the hydrophobic domains of PMHA effectively accommodated CXB, supporting its use as a codelivery nanoplatform for MEL and CXB. The release behavior of CXB from PMHA was investigated under both physiological (pH 7.3) and acidic (pH 5.0) conditions to mimic the extracellular and endosomal/lysosomal environments, respectively (Figure 1d). In both conditions, a biphasic release profile was observed, consisting of an initial burst phase within

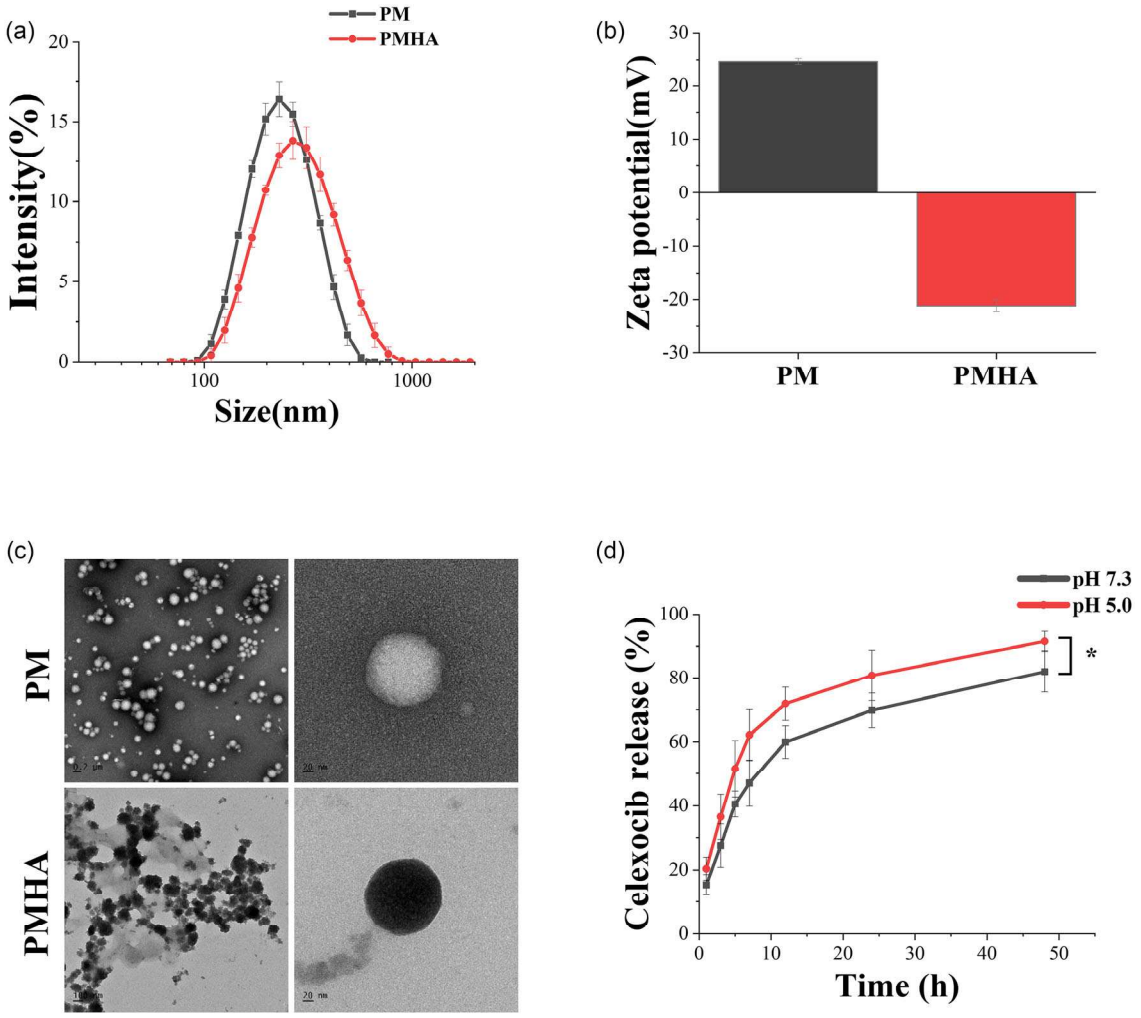


FIGURE 1 | Physicochemical characterization of PM and PMHA. (a) Hydrodynamic size distribution profiles determined by dynamic light scattering, demonstrating an increase in size upon HA coating. (b) Zeta potential measurements illustrating a surface charge inversion from positive (PM) to negative (PMHA) following HA functionalization. (c) Representative TEM images confirming the vesicular morphology of PM (top panels) and the enhanced surface contrast of PMHA (bottom panels), indicative of HA coating. Scale bars: left panels, 200 nm; right panels, 100 nm. (d) In vitro cumulative release profile of celecoxib (CXB) from PMHA in phosphate-buffered saline (PBS) at pH 7.3 and pH 5.0, measured at 37°C over 48 h. CXB concentrations were quantified by reverse-phase HPLC. Data are presented as mean ± SD, $n = 3$. Statistical significance between pH 7.3 and pH 5.0 at the indicated time point was determined using a two-sided unpaired Student's t-test. *$p < 0.05$.

18607187, 2026, 14, Downloaded from https://chemistry-europe.onlinelibrary.wiley.com/doi/10.1002/cmdc.70396 by Hyuncheol Kim - Sogang University , Wiley Online Library on [24/07/2026]. See the Terms and Conditions (https://onlinelibrary.wiley.com/terms-and-conditions) on Wiley Online Library for rules of use; OA articles are governed by the applicable Creative Commons License

TABLE 1 | Effect of HA coating ratio on hydrodynamic size (Z-average) and zeta potential of PM.

Formulations	Weight ratio PM:HA	Z-average, nm	Zeta potential, mV
PM	—	218.2 ± 1.7	+24.67 ± 0.6
PM/HA	1:2	265.5 ± 1.6	−21.14 ± 1.1
PM/HA	1:3	298.1 ± 8.1	−19.48 ± 0.6
PM/HA	1:4	1489.0 ± 78.0	−31.42 ± 0.3
PM/HA	1:8	1185.0 ± 19.8	−33.65 ± 0.05
PM/HA	1:10	633.2 ± 26.1	−31.96 ± 1.3

the first 12 h followed by a slower sustained release. At pH 7.3, approximately 68% of the encapsulated CXB was released within 24 h, reaching ~82% at 48 h. In contrast, the release rate was significantly accelerated at pH 5.0, with ~75% released at 24 h and ~92% at 48 h ($p < 0.05$).

This pronounced pH-dependent release suggests that PMHA can maintain stability under physiological conditions while enabling more efficient drug release in acidic intracellular compartments. Such behavior is advantageous for macrophage-targeted delivery, as CXB becomes more rapidly available once PMHA undergoes CD44-mediated endocytosis and traffics into endosomes and lysosomes. The faster release of CXB in acidic environments likely contributes to the enhanced suppression of COX-2 and TNF-α observed in functional assays, thereby coupling environmental responsiveness with improved therapeutic efficacy. Collectively, these findings confirm that the pH-sensitive release property of PMHA not only enhances intracellular drug availability but also minimizes premature release under normal physiological conditions, reinforcing its potential as a selective and effective nanoplatform for anti-inflammatory therapy.

2.14.3 | *Cell Viability and Hemolysis Assay of PM and PMHA*

MEL is recognized for its potent anti-inflammatory activities at low concentrations; however, its therapeutic utility is often constrained by significant hemolytic activity and cytotoxicity at higher, therapeutically relevant doses [28]. Therefore, a critical aspect of developing MEL-based therapeutics is to establish a safe and effective concentration range and to mitigate its inherent toxicities. To evaluate the in vitro cytocompatibility of our formulations, RAW 264.7 macrophages were treated with free MEL or PMHA at MEL-equivalent concentrations of 0.5, 1, and 2 μg/mL for 24 h, and cell viability was assessed using the MTT assay (Figure 2a). Treatment with free MEL resulted in a dose-dependent decrease in cell viability, with 90.26 ± 3.1%, 76.25 ± 4.5%, and 52.18 ± 5.2% of cells remaining viable at MEL concentrations of 0.5, 1, and 2 μg/mL, respectively. In contrast, cells treated with PMHA exhibited minimal cytotoxicity, maintaining high viabilities of 99.27 ± 2.5%, 98.74 ± 1.9%, and 97.21 ± 2.8% at the corresponding MEL-equivalent concentrations. This significant reduction in cytotoxicity highlights the protective effect of nanoparticle encapsulation. To further assess the safety of the formulations, particularly concerning MEL's well-documented membrane-disruptive activity, a hemolysis assay was performed using mouse RBCs. This assay quantifies the extent of hemoglobin release, an indicator of erythrocyte membrane damage. As depicted in Figure 2b, free MEL induced substantial hemolysis in a concentration-dependent manner, increasing from 10.81 ± 0.38% at 0.5 μg/mL to 100.00 ± 1.09% at 10 μg/mL. In contrast, PMHA markedly reduced MEL-associated hemolytic activity across the same concentration range, with hemolysis increasing from only 1.52 ± 0.28% at 0.5 μg/mL to 44.14 ± 2.61% at 10 μg/mL. Notably, at the biologically relevant MEL-equivalent concentration of 2 μg/mL, PMHA reduced hemolysis from 54.18 ± 3.34% for free MEL to 6.59 ± 1.34%. These results clearly indicate that

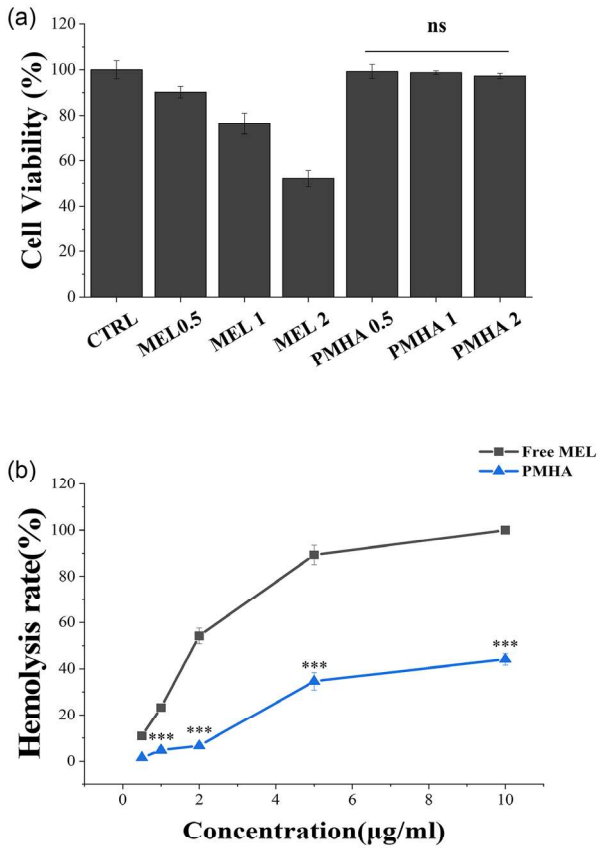


FIGURE 2 | In vitro cytocompatibility and hemolytic activity of free melittin (MEL) and PMHA. (a) Viability of RAW 264.7 macrophages after 24 h treatment with free MEL or PMHA at MEL-equivalent concentrations of 0.5, 1, and 2 μg/mL, assessed by MTT assay. Untreated cells served as the control group. Data are presented as mean ± SD, $n = 3$. (b) Hemolysis of mouse red blood cells after 6 h incubation with free MEL or PMHA at matched MEL-equivalent concentrations. Data are presented as mean ± SD, $n = 6$. Statistical significance between free MEL and PMHA at matched concentrations in panels (a) and (b) was determined using two-way ANOVA followed by Sidak multiple-comparisons test. ns, not significant; ***$p < 0.001$.

18607187, 2026, 14, Downloaded from https://chemistry-europe.onlinelibrary.wiley.com/doi/10.1002/cmdc.70396 by Hyuncheol Kim - Sogang University , Wiley Online Library on [24/07/2026]. See the Terms and Conditions (https://onlinelibrary.wiley.com/terms-and-conditions) on Wiley Online Library for rules of use; OA articles are governed by the applicable Creative Commons License

the encapsulation of MEL within the HA-coated polymersome structure, potentially stabilized by disulfide crosslinking within the polymersome membrane, effectively shields erythrocytes from MEL's lytic effects, thereby substantially improving its in vitro safety profile. Up to a MEL-equivalent concentration of 2 μg/mL, PMHA demonstrated minimal cytotoxicity to macrophages and negligible hemolytic activity, supporting its suitability for further biological evaluation and potential therapeutic applications.

2.14.4 | *In Vitro Cellular Uptake Studies*

Macrophages at inflamed sites overexpress CD44, a receptor for HA, which facilitates selective uptake of HA-functionalized nanocarriers [29, 30]. CD44 is particularly abundant on synovial macrophages in rheumatoid arthritis and has been linked to disease progression and severity [31]. To assess whether PMHA nanoparticles undergo CD44-mediated internalization, cellular uptake was examined by flow cytometry and confocal microscopy. RAW 264.7 macrophages were pretreated with an anti-CD44 monoclonal antibody (CD44 mAb) prior to incubation with Alexa Fluor 647–labeled PMHA (Figure 3a). Flow cytometry showed that CD44 blockade reduced mean fluorescence intensity (MFI) by ∼37.5% relative to unblocked controls (Figure 3b), indicating a major contribution of CD44 to PMHA uptake. Confocal microscopy further confirmed this finding: cells exposed to PMHA displayed strong intracellular fluorescence, whereas signal intensity was markedly reduced in CD44-blocked cells (Figure 3c). Collectively, these results demonstrate that PMHA are efficiently internalized by macrophages and that this process is substantially mediated by CD44, underscoring the role of HA functionalization in targeted delivery. The zeta-potential reversal from positive PM to negatively charged PMHA confirms the successful formation of an anionic HA corona on the polymersome surface. Although surface charge can influence nonspecific interactions with cell membranes, the enhanced uptake of PMHA is unlikely to be explained solely by electrostatic effects. In fact, the negative surface charge of HA-coated particles may reduce nonspecific membrane adsorption compared with cationic PM. The reduction in PMHA uptake after anti-CD44 antibody blocking indicates that HA–CD44 recognition is a major contributor to PMHA internalization. Therefore, charge reversal should be interpreted primarily as evidence of HA coating and improved ligand presentation, whereas CD44-mediated recognition is the dominant mechanism underlying targeted uptake.

2.14.5 | *Evaluation of TLR4 Expression After PMHA Treatment*

Toll-like receptors (TLRs) are pattern recognition receptors essential to innate immunity and are closely associated with autoimmune and inflammatory diseases [32]. Among these, TLR4 is prominently expressed on macrophages and, when activated by ligands such as bacterial LPS, initiates NF-κB signaling and induces proinflammatory cytokines [33]. Previous studies have reported that MEL can exert some of its anti-inflammatory effects by downregulating TLR4 expression or interfering with its signaling [34]. In contrast, nanoparticles are generally internalized via receptor-mediated endocytosis, allowing controlled intracellular release of their payloads [35]. Based on this distinction, we hypothesized that PMHA, unlike free MEL, would primarily enter macrophages through CD44-mediated endocytosis and release MEL intracellularly, rather than directly modulating TLR4. Accordingly, TLR4 mRNA levels were evaluated in LPS-treated RAW 264.7 macrophages after treatment with free MEL or PMHA at MEL-equivalent concentrations of 0.5, 1, and 2 μg/mL for 24 h. RT-PCR (Figure 3d) showed that free MEL caused a concentration-dependent downregulation of TLR4 mRNA, whereas PMHA produced no significant change across all concentrations, with levels comparable to the LPS control. These findings support the hypothesis that MEL is effectively shielded within PMHA until intracellular release, thereby avoiding premature interaction with surface TLR4. Together with the uptake studies, this indicates that CD44-mediated endocytosis is the predominant route for PMHA internalization in macrophages.

2.14.6 | *Suppression of Proinflammatory Mediator Expression by CXB/PMHA*

The anti-inflammatory effects of MEL, PMHA, and CXB/PMHA were evaluated in LPS-treated RAW 264.7 macrophages (Figure 4). LPS markedly increased COX-2 and TNF-α expression compared with untreated cells, confirming successful induction of an inflammatory state. COX-2 is a critical enzyme in the inflammatory cascade, responsible for prostaglandin synthesis, and its expression is strongly induced by cytokines such as IL-1 and TNF-α through NF-κB activation [36, 37]. Likewise, TNF-α is a pivotal cytokine that orchestrates inflammatory responses and contributes to the pathogenesis of autoimmune and inflammatory disorders [38]. As shown in Figure 4a, free MEL and CXB reduced COX-2 mRNA expression by approximately 46% and 58%, respectively, relative to the LPS-treated group. PMHA also reduced COX-2 mRNA expression by approximately 49%. Notably, CXB/PMHA achieved the most pronounced suppression, reducing COX-2 mRNA expression by approximately 79% and restoring the expression level close to the untreated baseline. For TNF-α (Figure 4b), MEL suppressed expression by ∼44%, CXB by ∼21%, and PMHA by ∼53%, whereas CXB/PMHA yielded the strongest effect (∼59%).

To determine whether this transcriptional suppression translated into functional inhibition, ELISA assays were performed (Figure 4c,d). As shown in Figure S1, both PMHA and CXB exhibited dose-dependent inhibitory effects, with CXB exerting stronger suppression of COX-2 at lower concentrations, whereas PMHA more effectively reduced TNF-α at higher concentrations. These patterns were consistent with the RT-PCR results. ELISA-based F_a analysis further supported these inhibitory effects. Based on the mean ELISA responses, PMHA produced fraction affected (F_a) values of 0.22 for COX-2 and 0.47 for TNF-α, whereas free CXB produced F_a values of 0.65 and 0.20, respectively. Notably, CXB/PMHA produced the greatest inhibition, with F_a values of 0.90 for COX-2 and 0.72 for TNF-α. CI analysis, calculated according to the median-effect principle of Chou and Talalay [24], further demonstrated synergistic inhibition, with CI values of 0.48 for COX-2 and 0.67 for TNF-α.

Taken together, these results reveal strong concordance between dose-dependent inhibitory profiles (Figure S1), mRNA suppression (Figure 4a,b), and protein-level inhibition (Figure 4c,d). CXB primarily exerts its anti-inflammatory activity via COX-2 inhibition, consistent with prior reports in LPS-treated macrophages [39], whereas MEL more directly attenuates TNF-α expression

18607187, 2026, 14, Downloaded from https://chemistry-europe.onlinelibrary.wiley.com/doi/10.1002/cmdc.70396 by Hyuncheol Kim - Sogang University , Wiley Online Library on [24/07/2026]. See the Terms and Conditions (https://onlinelibrary.wiley.com/terms-and-conditions) on Wiley Online Library for rules of use; OA articles are governed by the applicable Creative Commons License

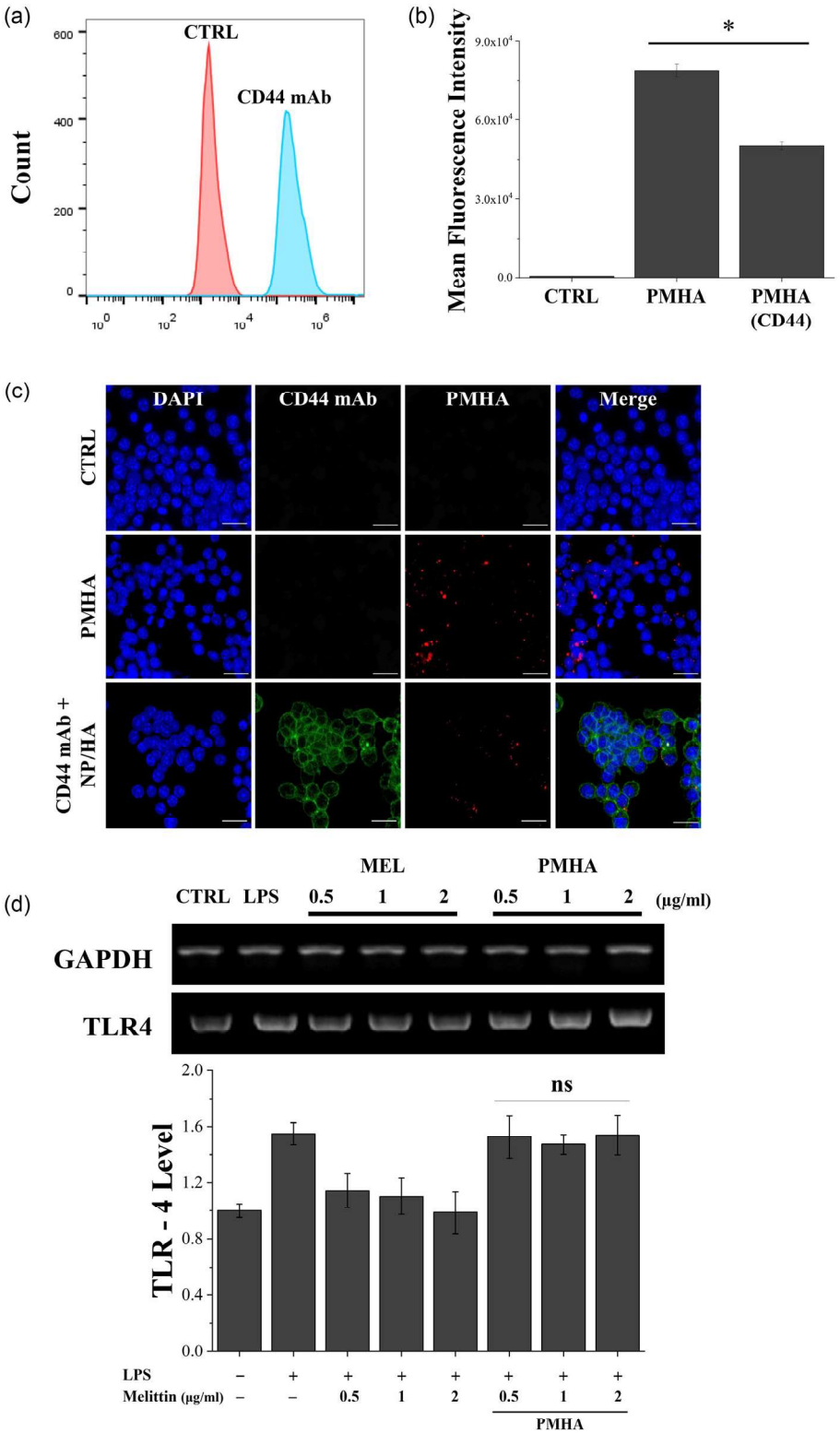


FIGURE 3 | CD44-mediated uptake and internalization pathway of PMHA in RAW 264.7 macrophages. (a) Flow cytometry histogram showing CD44 receptor expression on RAW 264.7 cells. (b) Quantitative analysis of Alexa Fluor 647-labeled PMHA uptake by flow cytometry in the absence or presence of CD44 monoclonal antibody blocking. Data are presented as mean ± SD, $n = 3$. Statistical significance was determined using a two-sided unpaired Student's t-test. *$p < 0.05$. (c) Representative confocal laser scanning microscopy images of Alexa Fluor 647-labeled PMHA internalization in RAW 264.7 cells treated with PMHA alone or pretreated with CD44 antibody; nuclei were counterstained with DAPI. Scale bar: 20 μm. (d) RT-PCR analysis of TLR4 mRNA expression in LPS-stimulated RAW 264.7 cells after 24 h treatment with free MEL or PMHA at MEL-equivalent concentrations of 0.5, 1, and 2 μg/mL; GAPDH served as the internal control. Data are presented as mean ± SD, $n = 3$. Statistical significance was determined using a two-sided unpaired Student's t-test for the indicated pairwise comparisons. ns, not significant; *$p < 0.05$.

18607187, 2026, 14, Downloaded from https://chemistry-europe.onlinelibrary.wiley.com/doi/10.1002/cmdc.70396 by Hyuncheol Kim - Sogang University , Wiley Online Library on [24/07/2026]. See the Terms and Conditions (https://onlinelibrary.wiley.com/terms-and-conditions) on Wiley Online Library for rules of use; OA articles are governed by the applicable Creative Commons License

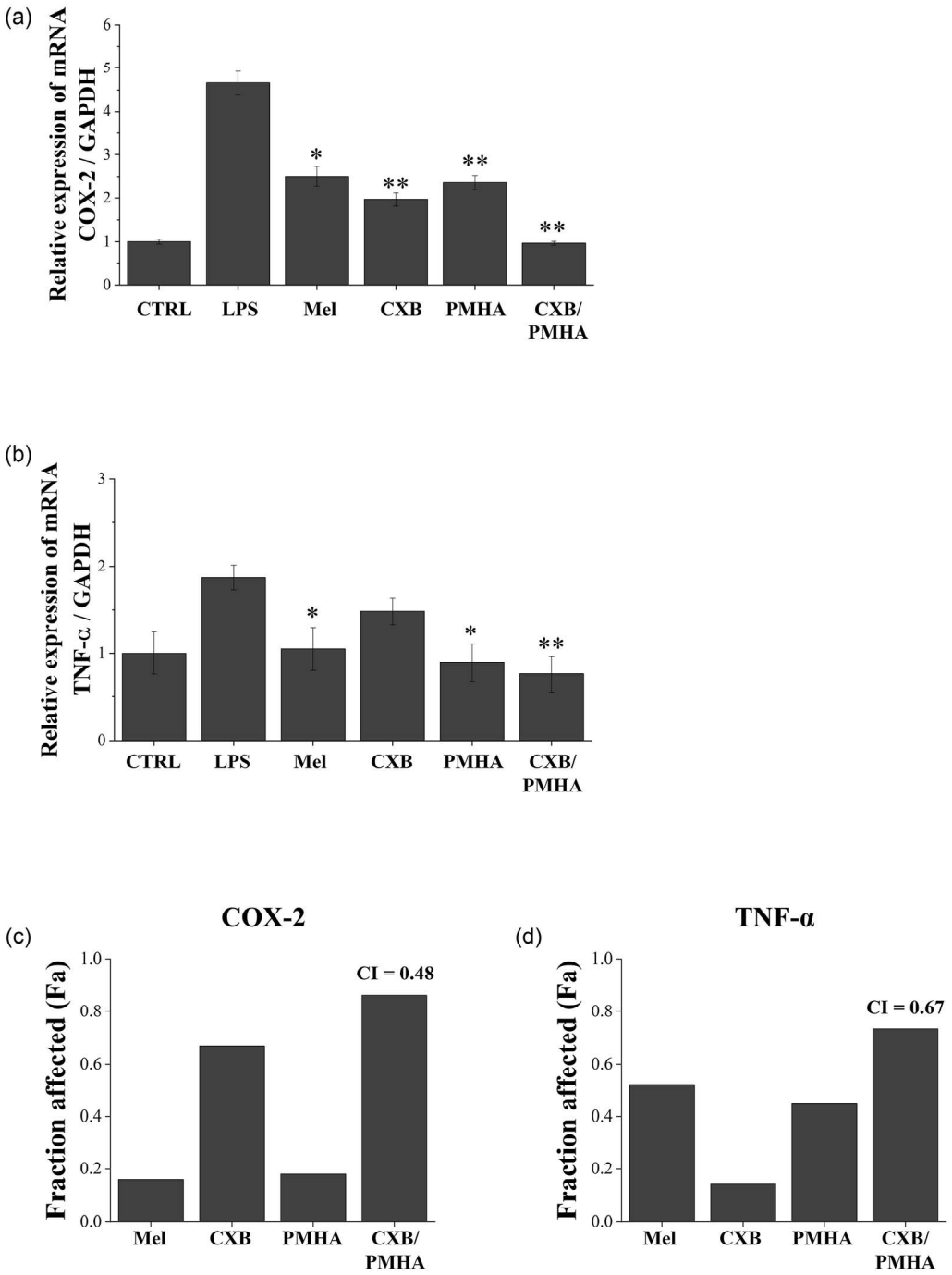


FIGURE 4 | Anti-inflammatory effects of MEL, CXB, PMHA, and CXB/PMHA on proinflammatory gene expression and mediator inhibition in LPS-stimulated RAW 264.7 macrophages. Cells were treated with MEL (2 μg/mL), CXB (1 μg/mL), PMHA (MEL-equivalent 2 μg/mL), or CXB/PMHA (MEL-equivalent 2 μg/mL and CXB 1 μg/mL) for 24 h after LPS-induced activation. (a) Relative mRNA expression of COX-2. (b) Relative mRNA expression of TNF-α. Gene expression was quantified by RT-PCR, normalized to GAPDH, and expressed relative to the indicated control group. Data in panels (a) and (b) are presented as mean ± SD, $n = 3$. Statistical significance was determined using one-way ANOVA followed by Tukey's multiple-comparisons test. ns, not significant; *$p < 0.05$; **$p < 0.01$. (c) Fraction affected (F_a) analysis of COX-2 protein levels measured by ELISA. (d) Fraction affected (F_a) analysis of TNF-α levels measured by ELISA. F_a values in panels (c) and (d) were calculated from the mean ELISA responses and are presented as calculated point estimates. Combination index (CI) values were calculated using the median-effect principle of Chou and Talalay.

by blocking NF-κB signaling, in line with earlier findings [11]. Their codelivery within the PMHA nanoplatform integrates these complementary mechanisms, resulting in synergistic downregulation of key inflammatory mediators and underscoring the promise of this system for the treatment of macrophage-driven inflammatory disease.

3 | Conclusion

PMHA was developed as a codelivery nanoplatform to provide both MEL, an active structural component, and CXB selectively to CD44-positive inflammatory macrophages. The vesicles exhibited nanoscale dimensions, confirmed HA surface adsorption,

18607187, 2026, 14, Downloaded from https://chemistry-europe.onlinelibrary.wiley.com/doi/10.1002/cmdc.70396 by Hyuncheol Kim - Sogang University , Wiley Online Library on [24/07/2026]. See the Terms and Conditions (https://onlinelibrary.wiley.com/terms-and-conditions) on Wiley Online Library for rules of use; OA articles are governed by the applicable Creative Commons License

and significantly reduced MEL-associated cytotoxicity. PMHA achieved high CXB loading with sustained release and was internalized through CD44-mediated endocytosis rather than direct TLR4 interaction. In LPS-treated RAW 264.7 cells, the codelivery system synergistically suppressed key proinflammatory markers, including COX-2 and TNF-α, outperforming free agents and single-component nanoparticles. These findings demonstrate that PMHA integrates targeted delivery with complementary anti-inflammatory mechanisms, offering a versatile nanoplatform for the treatment of macrophage-driven inflammatory diseases. While these in vitro results are promising, further in vivo studies will be conducted to evaluate the therapeutic efficacy and confirm the translational potential of PMHA.

Author Contributions

Youngheun Cho: conceptualization, methodology, investigation, data analysis, writing – original draft, writing – review and editing. **Junmin Kim**: investigation, data analysis. **Jooho Moon**: investigation, data analysis. **Soobin Nam**: investigation, data analysis. **Junhyung Kim**: investigation, data analysis. **Hyuncheol Kim**: supervision, funding acquisition, project administration, writing – review and editing.

Acknowledgments

A preliminary version of this work was presented at the KSBB-AFOB Conference 2025 by a member of our research group.

Funding

This research was supported by the Basic Science Research Program through the National Research Foundation of Korea (NRF), funded by the Ministry of Education, Science, and Technology (RS-2023-00261247, RS-2025-21 072 989), Republic of Korea and the Ministry of Food and Drug Safety grant (22213MFDS421), Republic of Korea.

Ethics Statement

No experiments involving human participants or live vertebrate animals were conducted in this study.

Conflicts of Interest

The authors declare no conflicts of interest.

Data Availability Statement

The datasets used and/or analyzed during the current study are available from the corresponding author on reasonable request.

References

1. R. Medzhitov, "Origin and Physiological Roles of Inflammation," *Nature* 454 (2008): 428–435.

2. C. A. Dinarello, "Proinflammatory Cytokines," *Chest* 118 (2000): 503–508.

3. P. Libby, "Inflammation in Atherosclerosis," *Arteriosclerosis, Thrombosis, and Vascular Biology* 32 (2012): 2045–2051.

4. C. Nathan, "Points of Control in Inflammation," *Nature* 420 (2002): 846–852.

5. G.-Q. Hou, C. Guo, G.-H. Song, et al., "Lipopolysaccharide (LPS) Promotes Osteoclast Differentiation and Activation by Enhancing the MAPK Pathway and COX-2 Expression in RAW. 264.7 Cells," *International Journal of Molecular Medicine* 32 (2013): 503–510.

6. G. Fan, X. Jiang, X. Wu, et al., "Anti-Inflammatory Activity of Tanshinone IIA in LPS-Stimulated RAW. 264.7 Macrophages via miRNAs and TLR4-NF-κB Pathway," *Inflammation* 39 (2016): 375–384.

7. K. Takeda and S. Akira, "TLR Signaling Pathways," *Seminars in Immunology* 16 (2004): 3–9.

8. G. S. Firestein, "Evolving Concepts of Rheumatoid Arthritis," *Nature* 423 (2003): 356–361.

9. H. Raghuraman and A. Chattopadhyay, "Melittin: A Membrane-Active Peptide with Diverse Functions," *Bioscience Reports* 27 (2007): 189–223.

10. H. J. Park, H. J. Lee, M. S. Choi, et al., "JNK Pathway Is Involved in the Inhibition of Inflammatory Target Gene Expression and NF-KappaB Activation by Melittin," *Journal of Inflammation* 5 (2008): 7.

11. H. J. Park, D. J. Son, C. W. Lee, et al., "Melittin Inhibits Inflammatory Target Gene Expression and Mediator Generation via Interaction with IκB Kinase," *Biochemical Pharmacology* 73 (2007): 237–247.

12. G. Gajski and V. Garaj-Vrhovac, "Melittin: A Lytic Peptide with Anticancer Properties," *Environmental Toxicology and Pharmacology* 36 (2013): 697–705.

13. X. Yu, Y. Dai, Y. Zhao, et al., "Melittin-Lipid Nanoparticles Target to Lymph Nodes and Elicit a Systemic Anti-Tumor Immune Response," *Nature Communications* 11 (2020): 1110.

14. L. Yang, F. Cui, K. Shi, D. Cun, and R. Wang, "Design of High Payload PLGA Nanoparticles Containing Melittin/Sodium Dodecyl Sulfate Complex by the Hydrophobic Ion-Pairing Technique," *Drug Development and Industrial Pharmacy* 35 (2009): 959–968.

15. J. E. Frampton and G. M. Keating, "Celecoxib: A Review of Its use in the Management of Arthritis and Acute Pain," *Drugs* 67 (2007): 2433–2472.

16. N. M. Davies, A. J. McLachlan, R. O. Day, and K. M. Williams, "Clinical Pharmacokinetics and Pharmacodynamics of Celecoxib: A Selective Cyclo-Oxygenase-2 Inhibitor," *Clinical Pharmacokinetics* 38 (2000): 225–242.

17. K. L. Goa and P. Benfield, "Hyaluronic Acid. A Review of Its Pharmacology and use as a Surgical Aid in Ophthalmology, and Its Therapeutic Potential in Joint Disease and Wound Healing," *Drugs* 47 (1994): 536–566.

18. S. Choi, W. Choi, S. Kim, S.-Y. Lee, I. Noh, and C.-W. Kim, "Purification and Biocompatibility of Fermented Hyaluronic Acid for Its Applications to Biomaterials," *Biomaterials Research* 18 (2014): 6.

19. B. P. Toole, "Hyaluronan: From Extracellular Glue to Pericellular Cue," *Nature Reviews Cancer* 4 (2004): 528–539.

20. S. Misra, V. C. Hascall, R. R. Markwald, and S. Ghatak, "Interactions between Hyaluronan and Its Receptors (CD44, RHAMM) Regulate the Activities of Inflammation and Cancer," *Frontiers in Immunology* 6 (2015): 201.

21. P. Johnson and B. Ruffell, "CD44 and Its Role in Inflammation and Inflammatory Diseases," *Inflammation & Allergy Drug Targets* 8 (2009): 208–220.

22. Y. Zhang, Q. Xia, Y. Li, et al., "CD44 Assists the Topical Anti-Psoriatic Efficacy of Curcumin-Loaded Hyaluronan-Modified Ethosomes: A New Strategy for Clustering Drug in Inflammatory Skin," *Theranostics* 9 (2019): 48–64.

23. S. De Bernardo, M. Weigele, V. Toome, et al., "Studies on the Reaction of Fluorescamine with Primary Amines," *Archives of Biochemistry and Biophysics* 163 (1974): 390–399.

24. T.-C. Chou and P. Talalay, "Quantitative Analysis of Dose-Effect Relationships: The Combined Effects of Multiple Drugs or Enzyme Inhibitors," *Advances in Enzyme Regulation* 22 (1984): 27–55.

25. D. E. Discher and F. Ahmed, "Polymersomes," *Annual Review of Biomedical Engineering* 8 (2006): 323–341.

26. A. Almalik, R. Donno, C. J. Cadman, F. Cellesi, P. J. Day, and N. Tirelli, "Hyaluronic Acid-Coated Chitosan Nanoparticles: Molecular Weight-Dependent Effects on Morphology and Hyaluronic Acid Presentation," *Journal of Controlled Release* 172 (2013): 1142–1150.

18607187, 2026, 14, Downloaded from https://chemistry-europe.onlinelibrary.wiley.com/doi/10.1002/cmdc.70396 by Hyuncheol Kim - Sogang University , Wiley Online Library on [24/07/2026]. See the Terms and Conditions (https://onlinelibrary.wiley.com/terms-and-conditions) on Wiley Online Library for rules of use; OA articles are governed by the applicable Creative Commons License

27. J. S. Lee and J. Feijen, "Polymersomes for Drug Delivery: Design, Formation and Characterization," *Journal of Controlled Release* 161 (2012): 473–483.

28. G. Lee and H. Bae, "Anti-Inflammatory Applications of Melittin, a Major Component of Bee Venom: Detailed Mechanism of Action and Adverse Effects," *Molecules* 21 (2016): 616.

29. R. W. Kinne, R. Bräuer, B. Stuhlmüller, E. Palombo-Kinne, and G. R. Burmester, "Macrophages in Rheumatoid Arthritis," *Arthritis Research* 2 (2000): 189–202.

30. Z. Szekanecz and A. E. Koch, "Macrophages and Their Products in Rheumatoid Arthritis," *Current Opinion in Rheumatology* 19 (2007): 289–295.

31. C. M. Isacke and H. Yarwood, "The Hyaluronan Receptor, CD44," *The International Journal of Biochemistry & Cell Biology* 34 (2002): 718–721.

32. K. Vijay, "Toll-Like Receptors in Immunity and Inflammatory Diseases: Past, Present, and Future," *International Immunopharmacology* 59 (2018): 391–412.

33. C. Vaure and Y. Liu, "A Comparative Review of Toll-Like Receptor 4 Expression and Functionality in Different Animal Species," *Frontiers in Immunology* 5 (2014): 316.

34. O. A. Ahmedy, S. M. Ibrahim, H. H. Salem, and E. A. Kandil, "Antiulcerogenic Effect of Melittin via Mitigating TLR4/TRAF6 Mediated NF-κB and p38MAPK Pathways in Acetic Acid-Induced Ulcerative Colitis in Mice," *Chemico-Biological Interactions* 331 (2020): 109276.

35. S. Zhang, J. Li, G. Lykotrafitis, G. Bao, and S. Suresh, "Size-Dependent Endocytosis of Nanoparticles," *Advanced Materials* 21 (2009): 419–424.

36. H.-Y. Yoon, E.-G. Lee, H. Lee, et al., "Kaempferol Inhibits IL-1β-Induced Proliferation of Rheumatoid Arthritis Synovial Fibroblasts and the Production of COX-2, PGE2 and MMPs," *International Journal of Molecular Medicine* 32 (2013): 971–977.

37. L. J. Crofford, "The Role of COX-2 in Rheumatoid Arthritis Synovial Tissues," *Arthritis Research* 1 (2000): S30.

38. R. W. Johnson, "Inhibition of Growth by pro-Inflammatory Cytokines: An Integrated View," *Journal of Animal Science* 75 (1997): 1244–1255.

39. Y. Pang, L. Gan, X. Wang, Q. Su, C. Liang, and P. He, "Celecoxib Aggravates Atherogenesis and Upregulates Leukotrienes in ApoE-/- Mice and Lipopolysaccharide-Stimulated RAW. 264.7 Macrophages," *Atherosclerosis* 284 (2019): 50–58.

Supporting Information

Additional supporting information can be found online in the Supporting Information section.

18607187, 2026, 14, Downloaded from https://chemistry-europe.onlinelibrary.wiley.com/doi/10.1002/cmdc.70396 by Hyuncheol Kim - Sogang University , Wiley Online Library on [24/07/2026]. See the Terms and Conditions (https://onlinelibrary.wiley.com/terms-and-conditions) on Wiley Online Library for rules of use; OA articles are governed by the applicable Creative Commons License